XV International Conference on Computational Plasticity. Fundamentals and Applications
COMPLAS 2019
E. Oñate, D.R.J. Owen, D. Peric, M. Chiumenti & Eduardo de Souza Neto (Eds)

SOME NUMERICAL VERIFICATION EXAMPLES FOR PLANE STRESS ELASTO-VISCOPLASTICITY

ANDREY BREZOLIN[†], TIAGO DOS SANTOS[††], PEDRO A. R. ROSA[†††] AND RODRIGO ROSSI[†]

[†]Departamento de Engenharia Mecânica, Universidade Federal do Rio Grande do Sul
Rua Sarmento Leite, 425, Porto Alegre, RS, 90046-902, Brazil
e-mail: andreybrezolin@gmail.com, rrossi@ufrgs.br

[†]Departamento de Engenharia Mecânica, Universidade Federal de Santa Maria
Av. Roraima, 1000, Prédio 7, Santa Maria, RS, 97105-900, Brazil
e-mail:tsantos.dem@smail.ufsm.br

[†††]Instituto de Engenharia Mecânica, Instituto Superior Técnico, Universidade de Lisboa
Lisboa, Portugal - 1049-001
e-mail: pedro.rosa@tecnico.ulisboa.pt

Key words: Verification examples, Viscoplastic material, Plane stress, Stress projected algorithms, Strain-rate hardening, Overstress function

Abstract. This paper presents analytical, semi-analytical and numerical reference examples which can be employed for code verification of elasto-viscoplastic models under plane stress conditions. Mainly because of the overstress function the algorithms traditionally employed in elasto-plastic implementations must be rewritten to correctly impose the plane stress state along with the viscoplastic flow. The viscoplastic formulation presented here considers the strain-rate hardening effects by means of a hardening law that are assumed to have terms depending on the strain rate, which removed can represent a Voce type hardening. The proposed verification tests were employed for the numerical verification of an in-house implementation of the so-called stress-projected procedure inside the finite element method context. Although the focus of this paper is on the stress-projected algorithms the examples presented here can be employed for the verification of other algorithms intended to impose the plane stress state in viscoplasticity.

1 INTRODUCTION

In many engineering practical applications, depending on specific physical and geometric characteristics, useful simplifications can be conveniently assumed. For example, either axisymmetric, plane strain or plane stress assumptions can be referred to. From a general point of view, such assumptions greatly simplifies the problem solution since a reduced number of variables has to be taken into account. Particularly, plane stress

conditions can be adopted in specific engineering situations in which, by suitable mathematical idealization, the out-of-plane stress components are assumed to be null. Practical applications which allow such an assumption are those involving e.g. thin membranes, load-free surfaces, etc.

Particularly, a straightforward formulation can be obtained when isotropic linear elasticity is employed. In this simple case, conditions satisfying null out-of-plane stress components are readily imposed both on analytical and numerical frameworks. In contrast to the linear elastic cases, imposing the corresponding plane stress conditions in inelastic formulations is more complex from both analytical and numerical points of views. It is worth mentioning that imposing the correct constraints to the plastic flow under plane stress assumption is far more complicated when compared to other simplifications, as axisymmetric or plane strain cases, or even when a full three dimensional approach is employed.

This paper focus on development of verification examples which can be applied especially for code verification involving viscoplasticity and in some conditions elasto-viscoplasticity problems. In a first moment, focus is given in some simple, but very important, verification examples in which numerical results are confronted against with analytical and semi-analytical rigid viscoplastic solutions. The term semi-analytical is used here to enforce that some approximation is involved in the development of the evolution of the viscoplastic flow. Secondly, it is presented some comparisons considering a more sophisticated plane stress example, also considered by other researches, serving as reference solutions.

In this paper the enforcement of the plane stress viscoplastic flow is given by a version of the *stress-project algorithm*. Although the stress-projected algorithm is very common in elasto-plasticity, the same does not appear to be true in elasto-viscoplasticity, and few papers on the subject are found in the literature, see subsection 3.2 for more details. The viscoplastic formulation is given in terms of an overstress function which couples viscid and inviscid flow. It is shown that to employ the stress-projected procedure some terms must arise in order to assure the correct evolution of the plane stress state along the viscoplastic flow. The elasto-viscoplastic model considered in this paper is equipped with an internal variable that accounts for the strain-rate hardening, which removed can lead to a Voce type of hardening, thus the procedure presented here can be employed when enforcing the plane stress state not only when using the stress-projected algorithm but also for other algorithms in regular viscoplastic models.

This paper is presented in a very concise manner in 6 sections, including this introduction. In section 2 the formulation of the elasto-viscoplastic constitutive model is briefly depicted. The formulation of the stress-projected algorithm is presented in section 3 and section 4 is devoted to the numerical aspects involved in the local integration procedure and tangent modulus derivation. Numerical results are presented in section 5. Closing this paper we present our conclusions in section 6.

2 CONSTITUTIVE FRAMEWORK

This section addresses the main features of the constitutive model and some important aspects associated with the plane stress particularization. In a first step, the adopted elasto-viscoplastic model is outlined. It is worth mentioning that this model was formulated and and adjusted within a multidimensional context in previous work [1]. The present development has the aim of emphasizing specific aspects related to both analytical and numerical formulations to employ the whole model (whose parameters were adjusted in a 3D setup) in a plane stress-projected framework.

2.1 Elasto-viscoplastic model

The model adopted in this work employs a von Mises material, whose yield function is given by

$$f(\boldsymbol{\sigma}, A) = \|\mathbf{s}\| - \underbrace{\sqrt{\frac{2}{3}}(\sigma_y + A)}_{R(A)}, \tag{1}$$

in which σ_y is the initial yield stress, $A = A_1 + A_2$ is the isotropic stress hardening, $||\mathbf{s}|| = \sqrt{\mathbf{s} : \mathbf{s}} = \sqrt{s_{ij} s_{ij}}$, being $\mathbf{s}$ the deviatoric part of the $\boldsymbol{\sigma}$. Assuming a linear elastic isotropic material, $\boldsymbol{\sigma}$ relates to an elastic strain measure $\boldsymbol{\varepsilon}^e$, by

$$\boldsymbol{\sigma} = \mathbf{D}^e \boldsymbol{\varepsilon}^e, \tag{2}$$

where

$$\mathbf{D}^e = 2\mu \mathbf{I} + \lambda \mathbf{I} \otimes \mathbf{I}, \tag{3}$$

being μ and λ the Lamé constants, which are related to standard elastic parameters as the shear G and bulk K moduli by $\mu = G$ and $\lambda = K - \frac{2}{3}\mu$. In Eq. (3), $\mathbf{I}$ is the *symmetric part* of the fourth order identity tensor, and $\mathbf{I}$ is the second order identity tensor. In components, they are given respectively by $\mathbf{I}_{ijkl} = \frac{1}{2}\left(\delta_{ik}\delta_{jl} + \delta_{il}\delta_{jk}\right)$ and $(\mathbf{I} \otimes \mathbf{I})_{ijkl} = \delta_{ij}\delta_{kl}$.

Inelastic evolution equations are given in the form

$$\dot{\boldsymbol{\varepsilon}}^{vp} = \dot{\lambda}\frac{\partial f}{\partial \boldsymbol{\sigma}} = \dot{\lambda}\frac{\mathbf{s}}{\|\mathbf{s}\|}, \;\; \dot{A}_1 = \delta\left(A_\infty - A_1\right)\dot{\bar{\varepsilon}}, \;\; A_2 = cA_\infty\bar{\varepsilon}, \tag{4}$$

where $\dot{\boldsymbol{\varepsilon}}^{vp} = \dot{\boldsymbol{\varepsilon}} - \dot{\boldsymbol{\varepsilon}}^e$ is the viscoplastic strain-rate, δ, A_∞ and c are model parameters, $\bar{\varepsilon}$ is the accumulated viscoplastic strain , whose rate is defined given by (see Eqs. (1) and (4))

$$\dot{\bar{\varepsilon}} = \sqrt{\frac{2}{3}}\,\|\dot{\boldsymbol{\varepsilon}}^{vp}\| = \sqrt{\frac{2}{3}}\dot{\lambda}. \tag{5}$$

For a constant strain-rate, from Eqs. $(4)_{2-3}$ a closed expression for the hardening variable $A = A_1 + A_2$ can be obtained

$$A = A_\infty\left[1 + c\bar{\varepsilon} - \exp\left(-\delta\bar{\varepsilon}\right)\right]. \tag{6}$$

Furthermore, the present model assumes rate-dependence on A_∞, as presented in [2], given by

$$A_\infty = [1 - \beta(\dot{\bar{\varepsilon}})] A_\infty^{lwr} + \beta(\dot{\bar{\varepsilon}}) A_\infty^{up}, \tag{7}$$

where A_∞^{lwr} and A_∞^{up} are model constants. Parameters $(\cdot)^{lwr}$ and $(\cdot)^{up}$ are related to a lower $\dot{\bar{\varepsilon}}_{lwr} \ll 1$ and an upper $\dot{\bar{\varepsilon}}_{up} \gg 1$ reference strain-rates, respectively. In Eq. (7), functions β, are given by

$$\beta(\dot{\bar{\varepsilon}}) = \left(\frac{\langle \dot{\bar{\varepsilon}} - \dot{\bar{\varepsilon}}_{lwr} \rangle}{\dot{\bar{\varepsilon}}_{up} - \dot{\bar{\varepsilon}}_{lwr}} \right)^{\xi}, \tag{8}$$

satisfying $\beta(\dot{\bar{\varepsilon}}_{lwr}) = 0$ and $\beta(\dot{\bar{\varepsilon}}_{up}) = 1$. The parameter $\xi > 0$ is a model constant. In the last equation, operator $\langle x \rangle = \frac{1}{2}(x + |x|)$ is the Macaulay bracket.

Within a viscoplastic framework, multiplier $\dot{\lambda} \geq 0$ of Eq. $(4)_1$ is assumed to have a relationship with the yield function f and hardening variable A given by a constitutive equation [3, 4]

$$\dot{\lambda} = \Theta(\langle f \rangle, A), \tag{9}$$

where $\Theta \geq 0$ is an overstress function complying with condition $\Theta(0, A) = 0$. Considering a viscoplastic loading, in which $f > 0$ and $\dot{\lambda} > 0$, the Eq. (9) can be rewritten as

$$f = \Theta^{-1}\left(\dot{\lambda}, A\right). \tag{10}$$

In this work, function Θ^{-1} is assumed to have the following specific form

$$f = R(A)\left[\left(1 + \vartheta\dot{\lambda}\right)^{1/m} - 1\right], \tag{11}$$

where $\vartheta > 0$ and $1/m > 0$ are constants. The Eq. 11 is a variation of the Perzyna model, [3, 4], and was proposed by [5].

3 ELASTO-VISCOPLASTICITY UNDER PLANE STRESS CONDITION

3.1 Some preliminaries

Let $\boldsymbol{\sigma} \in \mathcal{S}$ be the Cauchy stress tensor, $\mathcal{S}$ being the second-order symmetric tensor space satisfying $\dim[\mathcal{S}] = 6$. The plane stress condition may be stated by using the Cauchy traction vector, $\boldsymbol{t}$, as those sections planes, for a fixed unitary normal $\boldsymbol{n}$, where

$$\boldsymbol{t}(\boldsymbol{n}) = \boldsymbol{\sigma}\boldsymbol{n} = \boldsymbol{0}. \tag{12}$$

For the sake of simplification, let $\boldsymbol{n} = \boldsymbol{e}_3$ and let $\mathcal{S}^p \subset \mathcal{S}$ be conveniently defined as the stress vector subspace satisfying the planes stress constrains such that

$$\mathcal{S}^p = \{\boldsymbol{\sigma} \in \mathcal{S} | \sigma_{13} = \sigma_{23} = \sigma_{33} = 0\}, \tag{13}$$

where $\dim[\mathcal{S}^p] = 3$.

3.2 Plane stress in viscoplasticity

Appropriate procedures have been proposed in the literature to enforce the plane stress state in *elasto-plasticity* following either local or global procedures, see [6, Chap. 9] for a review. One of these approaches is plane stress-projection algorithm, apparently first reported in [7] but well developed in [8] and especially in [9] for a von Mises yield criterion.

Due to its complexity, the plane stress-projection has been employed mainly in works considering a J_2 yield function within elasto-plasticity, where there are "uncountable" works published so far, and also in viscoplasticity, but in contrast, here one founds very few works [10, 11, 12, 13]. Also, few works employing such strategy using other yield criteria are found [14, 15, 16]. From a full three-dimensional framework, [15, 16] have developed a general consistent projected return mapping algorithm for plane stress isotropic plasticity. They have shown that, in contrast to previous approaches [7, 8, 9, 14, 17], both the stress return algorithm and the consistent tangent operator can be obtained by particularizing the three dimensional formulation to a bi-dimensional stress space. However, for constitutive approaches not employing the von Mises yield function, obtaining the corresponding plane stress-projected formulation can become very complex or even impracticable. Thus, other procedures shall be recommended [6], [15] has pointed out that it could be limited to isotropic plasticity theories.

Now focusing in (elasto-)viscoplasticity, one of the first reports of plane stress state imposition in viscoplasticity was given by [11]. In this paper the authors follows the ideas presented in [9] to reformulate the so-called Robinson's viscoplastic model. More recently, in [12] an elastic–viscoplastic implicit integration algorithm was presented based on the ideas developed for elasto-plasticity. The algorithm was developed for three-dimensional stress states but can approach the plane stress state in viscoplasticity by introducing corrections in the implicit integration evolution equations. However, it is in [13] that a more comprehensive analysis about the imposition of the plane stress state in viscoplasticity is delivered. Different time integration schemes are investigated and compared in a constitutive formulation that considers isotropic and kinematic hardening and damage. The viscous effect is introduced by a power or an hyperbolic sine function.

3.2.1 Plane stress projection framework

In order to formulated the corresponding plane stress framework, the Voigt notation is conveniently adopted. Thus, constitutive relation given in Eq. (2) is rewritten as[1]

$$\begin{bmatrix} \sigma_{11} \\ \sigma_{22} \\ \sigma_{33} \\ \sigma_{23} \\ \sigma_{13} \\ \sigma_{12} \end{bmatrix} = \frac{E}{(1+\nu)(1-2\nu)} \begin{bmatrix} 1-\nu & \nu & \nu & 0 & 0 & 0 \\ \nu & 1-\nu & \nu & 0 & 0 & 0 \\ \nu & \nu & 1-\nu & 0 & 0 & 0 \\ 0 & 0 & 0 & \frac{1-2\nu}{2} & 0 & 0 \\ 0 & 0 & 0 & 0 & \frac{1-2\nu}{2} & 0 \\ 0 & 0 & 0 & 0 & 0 & \frac{1-2\nu}{2} \end{bmatrix} \begin{bmatrix} \varepsilon^e_{11} \\ \varepsilon^e_{22} \\ \varepsilon^e_{33} \\ \gamma^e_{23} \\ \gamma^e_{13} \\ \gamma^e_{12} \end{bmatrix}, \quad (14)$$

[1]Notice that $\boldsymbol{\sigma}$, $\boldsymbol{\varepsilon}^e$, $\mathbf{s}$ are second order tensors while $\boldsymbol{\sigma}$, $\boldsymbol{\varepsilon}^l$, and $\boldsymbol{s}$ are column matrices.

in which E and ν are the Young modulus and Poisson ratio, respectively. To impose the associated plane stress conditions, the in-plane stress components are assumed to be σ_{11}, σ_{22} and σ_{12} . Therefore, Eq. (14) reduces to

$$\begin{bmatrix} \sigma_{11} \\ \sigma_{22} \\ \sigma_{12} \end{bmatrix} = \frac{E}{1-\nu^2} \begin{bmatrix} 1 & \nu & 0 \\ \nu & 1 & 0 \\ 0 & 0 & \frac{1-\nu}{2} \end{bmatrix} \begin{bmatrix} \varepsilon^e_{11} \\ \varepsilon^e_{22} \\ \gamma^e_{12} \end{bmatrix} \rightarrow \boldsymbol{\sigma} = \mathbf{D}^e \boldsymbol{\varepsilon}^e, \tag{15}$$

with the out-of-plane strain component given by $\varepsilon^e_{33} = \frac{-\nu}{E}(\sigma_{11} + \sigma_{22})$. Seeking for a compact notation, a plane stress vector $\boldsymbol{\sigma} \in \mathcal{S}^p \subset \mathcal{S}$ is conveniently defined

$$\boldsymbol{\sigma} = [\sigma_{11}\ \sigma_{22}\ \sigma_{12}]^T. \tag{16}$$

Consistently, a strain vector is accordingly defined

$$\boldsymbol{\varepsilon}^l = [\varepsilon^l_{11}\ \varepsilon^l_{22}\ 2\varepsilon^l_{12}]^T, \tag{17}$$

where the superscript l has to be set depending on the deformation regime, elastic or inelastic. The out-of-plane component ε^l_{33} is left to be specified along the work.

Under plane stress conditions, following the previous notation, the deviatoric stress is assumed to belong to the vector subspace

$$\mathcal{S}^d = \{\mathbf{s} \in \mathcal{S} | \mathrm{s}_{13} = \mathrm{s}_{23} = 0,\ \mathrm{tr}\,(\mathbf{s}) = 0\}. \tag{18}$$

Being $\overline{\mathbf{P}}$ a linear mapping $\overline{\mathbf{P}} : \mathcal{S}^p \longrightarrow \mathcal{S}^d$, it is possible to determine the deviatoric stress vector performing

$$\boldsymbol{s} = \overline{\mathbf{P}}\boldsymbol{\sigma}\ , \tag{19}$$

where

$$\boldsymbol{s} = [s_{11}\ s_{22}\ s_{12}]^T, \tag{20}$$

and

$$\overline{\mathbf{P}} := \frac{1}{3}\begin{bmatrix} 2 & -1 & 0 \\ -1 & 2 & 0 \\ 0 & 0 & 3 \end{bmatrix}. \tag{21}$$

Note that the out of plane deviatoric stress is calculated as $s_{33} = -(s_{11} + s_{22})$. In a similar manner, the deviatoric strain vector, denoted by

$$\boldsymbol{\epsilon} = [\epsilon_{11}\ \epsilon_{22}\ 2\epsilon_{12}]^T, \tag{22}$$

with $\epsilon_{11} = \varepsilon_{11} - \frac{1}{3}\mathrm{tr}\,(\boldsymbol{\varepsilon})$ and $\epsilon_{22} = \varepsilon_{22} - \frac{1}{3}\mathrm{tr}\,(\boldsymbol{\varepsilon})$, can be obtained from the mapping

$$\boldsymbol{\epsilon} = \mathbf{P}\boldsymbol{\varepsilon}, \tag{23}$$

where

$$\mathbf{P} = \frac{1}{3}\begin{bmatrix} 2 & -1 & 0 \\ -1 & 2 & 0 \\ 0 & 0 & 6 \end{bmatrix}. \tag{24}$$

3.2.2 Viscoplastic considerations

When the plane stress condition is imposed, $\boldsymbol{\sigma} \in \mathcal{S}^p$ and $\boldsymbol{s} \in \mathcal{S}^d$, specialization of the yield function Eq. (1) reads

$$f_{ps}(\boldsymbol{\sigma}, A) = \sqrt{\frac{2}{3}\left(\sigma_{11}^2 + \sigma_{22}^2 - \sigma_{11}\sigma_{22} + 3\sigma_{12}^2\right)} - R(A), \tag{25}$$

which can be compactly rewritten using the operator $\mathbf{P}$ as

$$f_{ps}(\boldsymbol{\sigma}, A) = \sqrt{\boldsymbol{\sigma}^T \mathbf{P} \boldsymbol{\sigma}} - R(A)\ . \tag{26}$$

It is worth mentioning that, although they have a different functional form, both the yield functions defined in Eqs. (1) and (26) return the same numerical value for a given plane stress state. Thus, the viscoplastic equation defined in Eq. (11) can be readily applied in the plane stress formulation

$$\begin{aligned} f_{ps} &= \Theta^{-1}\left(\dot{\lambda}, A\right), \\ &= R(A)\left[\left(1 + \vartheta\dot{\lambda}\right)^{1/m} - 1\right], \end{aligned} \tag{27}$$

or

$$f_{ps} + R(A) = R(A)\left[\left(1 + \vartheta\dot{\lambda}\right)^{1/m}\right]. \tag{28}$$

Notice that the last equation is a direct particularization of the full viscoplastic function whose argument is the multiplier $\dot{\lambda}$ employing model parameters (ϑ, m) adjusted in a 3D context. However, in an effort to employ the 3D adjusted model in a particular plane stress implementation, attention is needed in the mathematical manipulation of the model equations. Following the procedure presented in [18], it is useful to rewrite Eq. (28) as

$$f_{ps} + R(A) = \sqrt{2\tilde{f}_{ps}\left(\boldsymbol{\sigma}\right)} = R(A)\left[\left(1 + \vartheta\dot{\lambda}\right)^{1/m}\right], \tag{29}$$

where $2\tilde{f}_{ps}\left(\boldsymbol{\sigma}\right) = \boldsymbol{\sigma}^T \mathbf{P} \boldsymbol{\sigma}$. Thus, the following relation is obtained

$$\tilde{f}_{ps} = \frac{1}{3}(\sigma_y + A)^2\left[\left(1 + \vartheta\dot{\lambda}\right)^{1/m}\right]^2. \tag{30}$$

Based on the plane stress restriction and according to the adopted Voigt notation, the evolution equation $(4)_1$ is rewritten as (see Eq. (26))

$$\dot{\boldsymbol{\varepsilon}}_{ps}^{vp} = \frac{1}{\sqrt{\boldsymbol{\sigma}^T \mathbf{P} \boldsymbol{\sigma}}}\dot{\lambda}\mathbf{P}\boldsymbol{\sigma}, \tag{31}$$

or in a convenient compact form as

$$\dot{\boldsymbol{\varepsilon}}_{ps}^{vp} = \dot{\tilde{\lambda}}\mathbf{P}\boldsymbol{\sigma}, \tag{32}$$

in which $\dot{\boldsymbol{\varepsilon}}_{ps}^{vp} = [\dot{\varepsilon}_{ps_{11}}^{vp} \; \dot{\varepsilon}_{ps_{22}}^{vp} \; 2\dot{\varepsilon}_{ps_{12}}^{vp}]^T$. Notice that in Eq. (32), since $\mathbf{P}\boldsymbol{\sigma}$ is not a unit vector, the multiplier $\dot{\tilde{\lambda}}$ does not represent the magnitude of $\dot{\boldsymbol{\varepsilon}}_{ps}^{vp}$. Therefore, $\dot{\tilde{\lambda}}$ is related to the original (3D) viscoplastic multiplier $\dot{\lambda}$ by means of

$$\dot{\tilde{\lambda}} = \frac{1}{\sqrt{\boldsymbol{\sigma}^T \mathbf{P} \boldsymbol{\sigma}}} \dot{\lambda} \; . \tag{33}$$

In this context, in view of Eqs. (5) and (33), the accumulated viscoplastic strain rate $\dot{\bar{\varepsilon}}$ can be given in terms of $\dot{\tilde{\lambda}}$ according to

$$\dot{\bar{\varepsilon}} = \dot{\tilde{\lambda}} \sqrt{\frac{2}{3} \boldsymbol{\sigma}^T \mathbf{P} \boldsymbol{\sigma}}. \tag{34}$$

Relation given in Eq. (33) is an important point to be highlighted in the present plane stress particularization. Keeping in mind that $\dot{\lambda}$ is the original argument of the 3D viscoplastic function given in Eq. (11), *it is not possible to simply replace* $\dot{\lambda}$ by $\dot{\tilde{\lambda}}$, in manner that

$$f_{ps} = R(A) \left[\left(1 + \vartheta \dot{\tilde{\lambda}} \right)^{1/m} - 1 \right].$$

If this direct replacement is done, the parameters adjusted in a 3D framework cannot be used within the plane stress particularization, otherwise unexpected results will be obtained.

4 NUMERICAL ASPECTS

4.1 Local integration algorithm

Once the constitutive equations under plane stress assumption have been obtained, this section outlines the incremental counterpart and the corresponding integration algorithm used to solve the numerical problem. Adopting a fully implicit integration (backward Euler) procedure, the whole time interval is subdivided into time increments $\Delta t = t_{n+1} - t_n$ and the time rate of each quantity $(\cdot)$ is calculated by an increment $\Delta(\cdot) \coloneqq (\cdot)_{n+1} - (\cdot)_n$, being $(\cdot)_{n+1}$ and $(\cdot)_n$ the values at instants t_{n+1} and t_n, respectively. In this sense, Eq. (34) becomes

$$\bar{\varepsilon}_{n+1} = \bar{\varepsilon}_n + \Delta\tilde{\lambda} \sqrt{\frac{2}{3} \boldsymbol{\sigma}_{n+1}^T \mathbf{P} \boldsymbol{\sigma}_{n+1}}, \tag{35}$$

in which $\Delta\tilde{\lambda} \geq 0$ plays the role of a incremental viscoplastic multiplier.

Considering a viscoplastic loading $\left(f_{ps_{n+1}} > 0\right)$, based on Eq. (29) the following particular plane stress relation is obtained

$$\tilde{f}_{ps} = \frac{1}{2} \boldsymbol{\sigma}_{n+1}^T \mathbf{P} \boldsymbol{\sigma}_{n+1} - \frac{1}{3} (\sigma_y + A_{n+1})^2 \left(1 + \vartheta \frac{\Delta\tilde{\lambda}}{\Delta t} \sqrt{\boldsymbol{\sigma}_{n+1}^T \mathbf{P} \boldsymbol{\sigma}_{n+1}} \right)^{2/m} = 0. \tag{36}$$

In addition, the stress hardening variable A at t_{n+1} can be accounted for by means of the following incremental equation obtained from Eqs. $(4)_{2-3}$ (see also [1])

$$A_{n+1} = A_n + A_{\infty_{n+1}} c(\bar{\varepsilon}_{n+1} - \bar{\varepsilon}_n) + \\ + \left[A_{\infty_{n+1}}(1 + c\bar{\varepsilon}_n) - A_n\right] \left\{1 - \exp\left[-\delta(\bar{\varepsilon}_{n+1} - \bar{\varepsilon}_n)\right]\right\}, \quad (37)$$

in which $A_{\infty_{n+1}}$ is given by

$$A_{\infty_{n+1}} = A_\infty^{lwr} + \left[\frac{1}{\Delta t}\left(\frac{\langle \bar{\varepsilon}_{n+1} - \bar{\varepsilon}_n - \Delta t \dot{\bar{\varepsilon}}_{lwr} \rangle}{\dot{\bar{\varepsilon}}_{up} - \dot{\bar{\varepsilon}}_{lwr}}\right)\right]^\xi (A_\infty^{up} - A_\infty^{lwr}) \, . \quad (38)$$

4.1.1 Elastic predictor-plastic corrector algorithm in plane stress state

In order to solve the set of nonlinear algebraic equations (35)-(38), an elastic predictor-plastic corrector algorithm is employed. The strategy solution is performed into two steps: **(i)** a trial elastic state is assumed, if the condition $f_{ps}(\boldsymbol{\sigma}_{n+1}^{trial}, A_{n+1}^{trial}) \leq 0$ is satisfied, the solution at t_{n+1} is updated, $(\cdot)_{n+1} = (\cdot)_{n+1}^{trial}$; **(ii)** otherwise, if $f_{ps}(\boldsymbol{\sigma}_{n+1}^{trial}, A_{n+1}^{trial}) > 0$, a viscoplastic correction has to be performed. The elastic deformation for plane stress state, at t_{n+1}, can be written as

$$\boldsymbol{\varepsilon}_{n+1}^e = \boldsymbol{\varepsilon}_{n+1}^{e^{trial}} - \Delta\tilde{\lambda}\mathbf{P}\boldsymbol{\sigma}_{n+1}, \quad (39)$$

or equivalently in term of stresses

$$\boldsymbol{\sigma}_{n+1} = \mathbf{H}\left(\Delta\tilde{\lambda}\right)\boldsymbol{\sigma}_{n+1}^{trial}, \quad (40)$$

in which

$$\mathbf{H}\left(\Delta\tilde{\lambda}\right) = \left(\mathbf{D}^{e^{-1}} + \Delta\tilde{\lambda}\mathbf{P}\right)^{-1}\mathbf{D}^{e^{-1}}. \quad (41)$$

The nonlinear set of equations to be solved in the plastic corrector phase is composed by (35), (36), (37), (38), and (39) for the following variables $\left\{\boldsymbol{\varepsilon}_{n+1}^e, \bar{\varepsilon}_{n+1}, \Delta\tilde{\lambda}, A_{n+1}, A_{\infty_{n+1}}\right\}$. It is possible to reduce the number of equations by a simple mathematical manipulation of Eq. 36 and Eq. (39) (or Eq. (40)). These last two equations can be reduced to one equation having as unknown $\Delta\tilde{\lambda}$. To perform such a task let us first write

$$\boldsymbol{\sigma}_{n+1}^T\mathbf{P}\boldsymbol{\sigma}_{n+1} = \gamma\left(\Delta\tilde{\lambda}\right) \, , \quad (42)$$

where the function $\gamma\left(\Delta\tilde{\lambda}\right)$ is given in terms of the trial state as

$$\gamma\left(\Delta\tilde{\lambda}\right) = \left(\boldsymbol{\sigma}_{n+1}^{trial}\right)^T\mathbf{H}^T\left(\Delta\tilde{\lambda}\right)\mathbf{P}\mathbf{H}\left(\Delta\tilde{\lambda}\right)\boldsymbol{\sigma}_{n+1}^{trial}. \quad (43)$$

Previous equation has to be solved in terms of a single scalar unknown: $\Delta\tilde{\lambda}$. However, as pointed out by [6], given the fact that Eq. (43) involves the multiplication and inversion of

other matrices, its solution can lead to a cumbersome calculation. Therefore, in an effort to avoid such operations one can take the advantage of specific characteristic associated with an elastic and isotropic material. That means $\mathbf{P}$ and $\mathbf{D}^e$ share the same eigenvectors, i.e. both have diagonal representation on the same basis, as well as $\mathbf{D}^{e^{-1}}$ and $\mathbf{H}$. The orthogonal matrix $\mathbf{Q}$ representing such transformation is

$$\mathbf{Q} = \begin{bmatrix} \frac{1}{\sqrt{2}} & \frac{1}{\sqrt{2}} & 0 \\ -\frac{1}{\sqrt{2}} & \frac{1}{\sqrt{2}} & 0 \\ 0 & 0 & 1 \end{bmatrix}, \tag{44}$$

implying in the following results

$$\mathbf{P}^* \equiv \mathbf{Q}\mathbf{P}\mathbf{Q}^T = \begin{bmatrix} \frac{1}{3} & 0 & 0 \\ 0 & 1 & 0 \\ 0 & 0 & 2 \end{bmatrix}, \tag{45}$$

$$\mathbf{D}^{e*} \equiv \mathbf{Q}\mathbf{D}^e\mathbf{Q}^T = \begin{bmatrix} \dfrac{E}{1-\nu} & 0 & 0 \\ 0 & 2G & 0 \\ 0 & 0 & G \end{bmatrix}, \tag{46}$$

$$\begin{aligned} \mathbf{H}^*\left(\Delta\tilde{\lambda}\right) &\equiv \left(\mathbf{D}^{*e^{-1}} + \Delta\tilde{\lambda}\mathbf{P}^*\right)^{-1}\mathbf{D}^{*e^{-1}} \\ &= \begin{bmatrix} \dfrac{3(1-\nu)}{3(1-\nu)+E\Delta\tilde{\lambda}} & 0 & 0 \\ 0 & \dfrac{1}{1+2G\Delta\tilde{\lambda}} & 0 \\ 0 & 0 & \dfrac{1}{1+2G\Delta\tilde{\lambda}} \end{bmatrix}, \end{aligned} \tag{47}$$

and the trial stress can be written as

$$\boldsymbol{\sigma}_{n+1}^{trial^*} \equiv \mathbf{Q}\boldsymbol{\sigma}_{n+1}^{trial} = \begin{bmatrix} \frac{1}{\sqrt{2}}\left(\sigma_{11}^{trial} + \sigma_{22}^{trial}\right) \\ \frac{1}{\sqrt{2}}\left(\sigma_{22}^{trial} - \sigma_{11}^{trial}\right) \\ \sigma_{12}^{trial} \end{bmatrix}, \tag{48}$$

and Eq. (43) is rewritten as

$$\begin{aligned} \boldsymbol{\sigma}_{n+1}^T\mathbf{P}\boldsymbol{\sigma}_{n+1} &= \gamma\left(\Delta\tilde{\lambda}\right) \\ &= \frac{\left(\sigma_{11}^{trial} + \sigma_{22}^{trial}\right)^2}{6\left[1 + \dfrac{E\Delta\tilde{\lambda}}{3(1-\nu)}\right]^2} + \frac{\frac{1}{2}\left(\sigma_{22}^{trial} - \sigma_{11}^{trial}\right)^2 + 2\left(\sigma_{12}^{trial}\right)^2}{\left(1 + 2G\Delta\tilde{\lambda}\right)^2} \end{aligned} \tag{49}$$

The matrix $\mathbf{H}\left(\Delta\tilde{\lambda}\right)$ may be now written as

$$\mathbf{H}\left(\Delta\tilde{\lambda}\right) = \mathbf{Q}^T\mathbf{H}^*\left(\Delta\tilde{\lambda}\right)\mathbf{Q}, \tag{50}$$

and using Eq. (44) and (47), one can derive a simpler form as

$$\mathbf{H}(\Delta\tilde{\lambda}) = \begin{bmatrix} \frac{1}{2}(H^*_{11}+H^*_{22}) & \frac{1}{2}(H^*_{11}-H^*_{22}) & 0 \\ \frac{1}{2}(H^*_{11}-H^*_{22}) & \frac{1}{2}(H^*_{11}+H^*_{22}) & 0 \\ 0 & 0 & H^*_{33} \end{bmatrix}, \tag{51}$$

in which

$$H^*_{11} = \frac{3\,(1-\nu)}{3\,(1-\nu)+E\Delta\tilde{\lambda}},\; H^*_{22} = \frac{1}{1+2G\Delta\tilde{\lambda}},\; H^*_{33} = H^*_{22}. \tag{52}$$

It is also possible rewrite Eq. (35) and (36) in terms of $\Delta\tilde{\lambda}$ only, that is

$$\frac{1}{2}\gamma\left(\Delta\tilde{\lambda}\right) - \frac{1}{3}(\sigma_y + A_{n+1})^2\left[1+\vartheta\frac{\Delta\tilde{\lambda}}{\Delta t}\sqrt{\gamma\left(\Delta\tilde{\lambda}\right)}\right]^{2/m} = 0, \tag{53}$$

and

$$\bar{\varepsilon}_{n+1} = \bar{\varepsilon}_n + \Delta\tilde{\lambda}\sqrt{\frac{2}{3}\gamma\left(\Delta\tilde{\lambda}\right)}. \tag{54}$$

Moreover, by substituting Eq. (54) in Eqs. (37) and (38) one writes

$$\begin{aligned} A_{n+1} = A_n + A_{\infty_{n+1}} c\left[\Delta\tilde{\lambda}\sqrt{\frac{2}{3}\gamma\left(\Delta\tilde{\lambda}\right)}\right] + \\ + \left[A_{\infty_{n+1}}\left(1+c\bar{\varepsilon}_n\right) - A_n\right]\left\{1-\exp\left[-\delta\Delta\tilde{\lambda}\sqrt{\frac{2}{3}\gamma\left(\Delta\tilde{\lambda}\right)}\right]\right\}, \end{aligned} \tag{55}$$

with

$$A_{\infty_{n+1}} = A^{lwr}_{\infty} + \left[\frac{1}{\Delta t}\frac{\left\langle \Delta\tilde{\lambda}\sqrt{\frac{2}{3}\gamma\left(\Delta\tilde{\lambda}\right)} - \Delta t\dot{\bar{\varepsilon}}_{lwr}\right\rangle}{\dot{\bar{\varepsilon}}_{up}-\dot{\bar{\varepsilon}}_{lwr}}\right]^{\xi}\left(A^{up}_{\infty}-A^{lwr}_{\infty}\right). \tag{56}$$

In conclusion, the system of nonlinear equations related to the viscoplastic prediction phase is (53), (55), and (56) which has to be solved in terms of $\left\{\Delta\tilde{\lambda},\, A_{n+1},\, A_{\infty_{n+1}}\right\}$.

Consequently, once the solution is obtained, the stress $\boldsymbol{\sigma}_{n+1}$ and elastic strain $\boldsymbol{\varepsilon}^{e}_{n+1}$ are updated respectively as (see Eq. (40))

$$\boldsymbol{\sigma}_{n+1} = \mathbf{H}\left(\Delta\tilde{\lambda}\right)\boldsymbol{\sigma}^{trial}_{n+1},$$

and

$$\boldsymbol{\varepsilon}^{e}_{n+1} = \mathbf{D}^{e^{-1}}\boldsymbol{\sigma}_{n+1}.$$

4.2 Viscoplastic tangent operator for plane stress state

The viscoplastic tangent operator for plane stress state shall be derived $\mathbf{D}^{vp}_{ps}$ from the linearization of equations (36), (39), and (55). After a straightforward mathematical manipulation of this algebraic equations one identifies

$$\mathbf{D}^{vp}_{ps} = \frac{\partial\boldsymbol{\sigma}_{n+1}}{\partial\boldsymbol{\varepsilon}^{e^{trial}}_{n+1}} = \left[\mathbf{D}^{e^{-1}} + \frac{\mathbf{P}\boldsymbol{\sigma}_{n+1}\otimes\mathbf{P}\boldsymbol{\sigma}_{n+1}}{-\left(a_0\dfrac{\partial\tilde{f}_{ps}}{\partial A_{n+1}} + \dfrac{\partial\tilde{f}_{ps}}{\partial\Delta\tilde{\lambda}}\right)} + \Delta\tilde{\lambda}\mathbf{P}\right]^{-1}, \tag{57}$$

where

$$\begin{aligned} a_0 = \Big\{\delta\exp\left(-a_1\delta\Delta\tilde{\lambda}\right)\left[A_{\infty_{n+1}}\left(1+c\bar{\varepsilon}_n\right) - A_n\right] + \\ + A_{\infty_{n+1}}c\Big\}\left(a_1 + \frac{\Delta\tilde{\lambda}}{3a_1}\frac{\partial\gamma}{\partial\Delta\tilde{\lambda}}\right) + \\ + \left\{ca_1\Delta\tilde{\lambda} + \left(1+c\bar{\varepsilon}_n\right)\left[1-\exp\left(-\delta a_1\Delta\tilde{\lambda}\right)\right]\right\}\frac{\partial A_{\infty_{n+1}}}{\partial\Delta\tilde{\lambda}}, \end{aligned} \tag{58}$$

and

$$a_1 = \sqrt{\frac{2}{3}\gamma\left(\Delta\tilde{\lambda}\right)}. \tag{59}$$

5 NUMERICAL RESULTS

This section has the aim to assess the corresponding constitutive and numerical aspects associated with the present development. In this respect, with a view to evaluating the whole finite element framework, simple cases, such as uniaxial tension, simple shear and biaxial stretching, are simulated. Obtained numerical solutions are then compared to specific analytical solutions. A more detailed explanation on the derivation of the analytical and semi-analytical solutions employed in this section is presented in [19]. Comparisons consider strain-rates ranging from $10^{-2}\,\mathrm{s}^{-1}$ to $10^{4}\,\mathrm{s}^{-1}$. In the sequence, in order to evaluate the present approach considering the structural response of more complex problem with a non-homogeneous deformation field, the stretching of a perforated plate is also

simulated. Since this case has been considered in the literature, the present framework is adapted to reproduce the same constitutive formulation proposed in the works in literature allowing the comparison of the results with previous researches. After the numerical verification of the present proposal, specific constitutive features associated with the constitutive model employed herein can be further explored. For example, the strain-induced hardening which is expected to play a major role during the high rate loading of metallic materials. Thereby, specific simulations considering strain-rate hardening effects in plane stress conditions are finally performed.

5.1 Monoelements - Homogeneous results

The material parameters to be employed in the following analysis are those adjusted by [2], where annealed OFHC cooper samples were considered. Parameters values are presented in Table 1. A standard Newton-Raphson method was employed for the numerical solution of the nonlinear system of equations in the returning mapping phase. The minimum error tolerance for the residue norm of 10^{-6} was employed. All the analysis in this subsection were carried out considering a fixed number of iterations in time of $N = 20$ but varying the rates of deformation K.

Table 1: Material properties and model parameters for annealed OFHC cooper, with $\dot{\bar{\varepsilon}}_{lwr} = 10^{-4}$ s^{-1} and $\dot{\bar{\varepsilon}}_{up} = 10^{4}$ s^{-1}. Source: [2]

E (GPa)	ν	σ_y (MPa)	δ	c	A_∞^{lwr} (MPa)	A_∞^{up} (MPa)	ξ	ϑ (s)	m
112	0.33	35	6.46	0.42	233	420	3.16	1.2×10^3	105

5.1.1 Homogeneous compression

The problem addressed in this section consists in the solution of the application of a homogeneous compression in a geometry with quadrilateral shape where the plane stress state is imposed. The analyzed numerical model is formed by a single quadrilateral element of equal side $l_0 = 6$ mm of four nodes. The geometry and boundary conditions are presented in Fig. 1. Also, just for sake of comparison, a single brick element was also considered for analysis aiming to show that under the conditions specified in Fig. 1 the multiaxial element will reproduce the plane stress state and the results have to remain the same.

The analysis was performed by imposing a total homogeneous compression deformation of $\varepsilon_{22_f} = -0.5$ at the final time t_f, which is obtained by applying a total prescribed displacement of $\bar{u}_2 = -2.3608$ mm on the upper face of the element in Fig. 1. The analytical response was derived considering the condition of a rigid-viscoplastic material, resulting in the following stress evolution equation

$$|\sigma_{22}| = (\sigma_y + A)\left(1 + \sqrt{\frac{3}{2}}\vartheta|K|\right)^{1/m} . \tag{60}$$

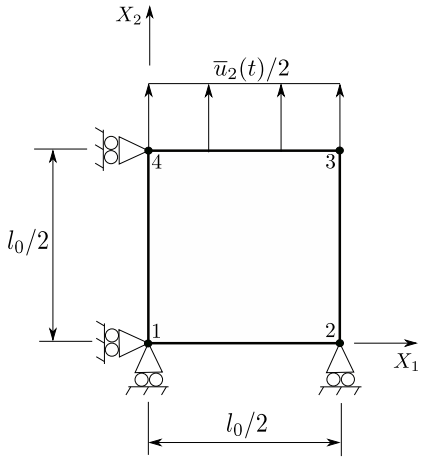

Figure 1: Homogeneous compression - Finite element mesh and boundary conditions.

The comparisons for the stress evolution and hardening evolution for different deformation rates are presented in Figs. 2 and 3. While analyzing the results of these figures it is clear that there is a good approximation between the numerical results with respect to the analytical solution. Due to the rigid-viscoplastic analytical solution, a slight deviation between numerical and analytical response is evidenced at earlier deformation stages. This difference is explained due to the significant contribution of the elastic deformation part at the beginning of the deformation process, which is not taken into account in the rigid viscoplastic analytical model.

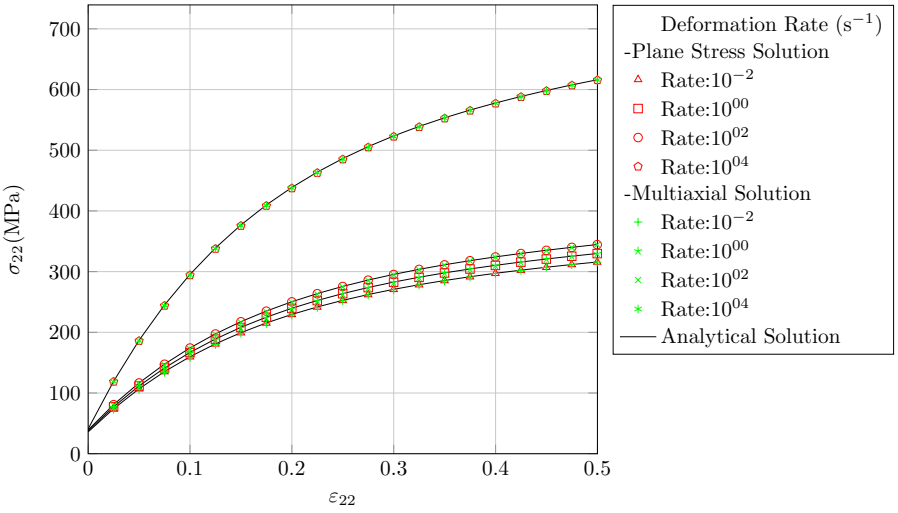

Figure 2: Comparison of flow stress-strain results for homogeneous compression.

It is also possible to observe that in the comparison between responses for the multiaxial stress state and for the plane stress state the result found also agrees with the expected response. Thus, the result indicates that the models developed respect the hypothesis that in the plane, for a given field of homogeneous strain/stress, the stress responses between

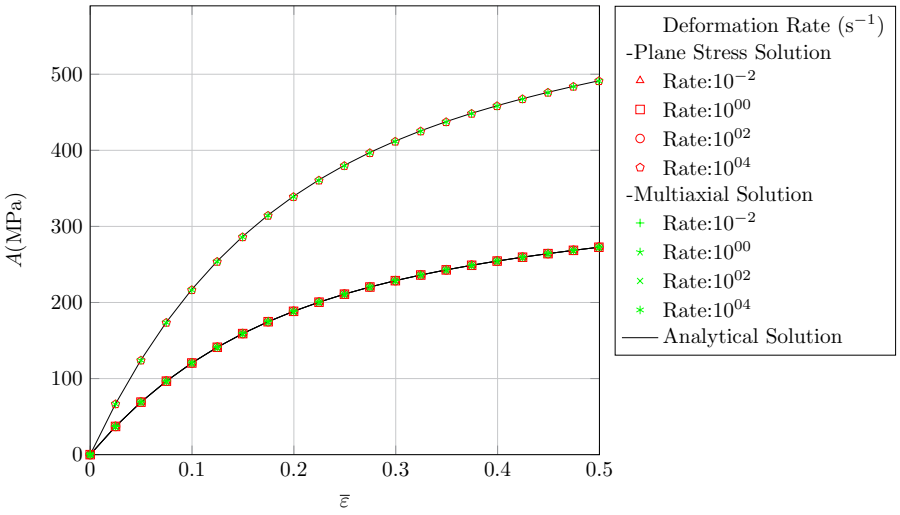

Figure 3: Comparison of hardening versus accumulated viscoplastic strain for homogeneous compression.

both cases must be the same.

5.1.2 Simple Shear

Here, we seek to find the same characteristics mentioned in the previous section, but now in front of a problem where the shear components are preponderant with respect to the normal components. The numerical model is formed by a single quadrilateral element of equal side $l_0 = 6$ mm of eight nodes. Figure 4 shows the geometry and boundary conditions employed for this example. A brick element was also considered for the multiaxial response.

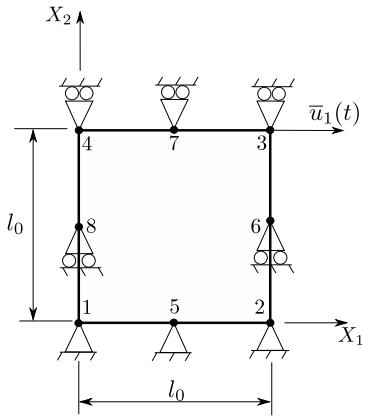

Figure 4: Simple shear - Finite element mesh and boundary conditions.

A total shear deformation of $2\varepsilon_{12} = 0.5$ at final time t_f was imposed, obtained from a prescribed displacement of $\overline{u}_1 = 3.124$ mm on the upper face of the element in Fig.

4. For this case, the developed approximate[2] response for the stress evolution, also for a rigid-viscoplastic material, is

$$|\sigma_{12}| = \sqrt{\frac{1}{3}}(\sigma_y + A)\left(1 + \frac{1}{\sqrt{2}}\vartheta|K|\right)^{1/m} . \tag{61}$$

Figures 5 and 6 show the evolution of the in-plane shear stress component versus the shear deformation and of the hardening in terms of the accumulated viscoplastic strain, respectively. Notice that, as for the first case, there is a very good agreement among the results.

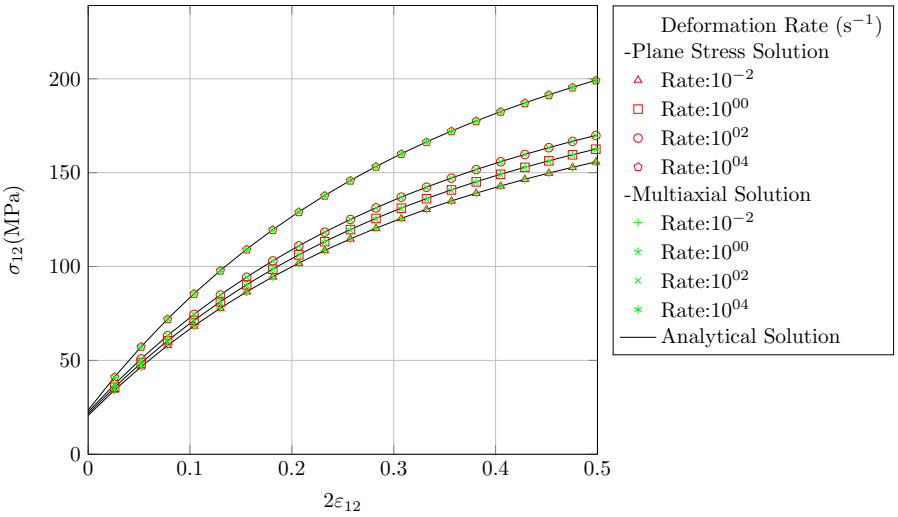

Figure 5: Comparison of flow stress-strain results for simple shear.

5.1.3 Biaxial stretching with finite rotation

The case analyzed in this section consists in the application of a simultaneous biaxial stretching and finite rotation on a single four node quadrilateral finite element of size $l_0 = 1$ mm, as depicted in Fig. 7 where the geometry and boundary conditions are presented. The biaxial stretching occurs in the X_1-X_2 plane while the rotation is around the X_3 axis.

The displacement field applied for this case is given by

$$\bar{u}_1 = \varpi X_2 \quad \text{and} \quad \bar{u}_2 = -\varpi X_1 . \tag{62}$$

At the final time the multiplier assumes the value of $\varpi = 0.7013$ resulting in a homogeneous deformation state of 0.5.

[2]During the development of the analytical solution, under finite deformation, the normal stress components were considered small with relation to the shear component. Therefore the normal components were disregarded.

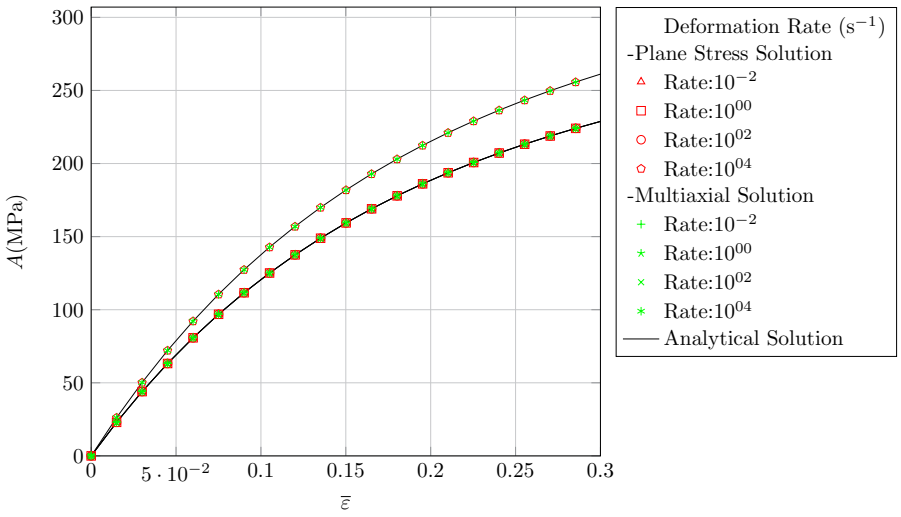

Figure 6: Comparison of hardening versus accumulated viscoplastic strain for simple shear.

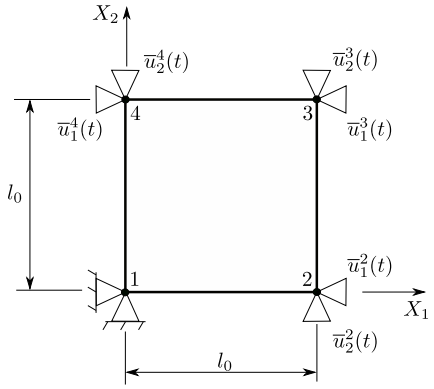

Figure 7: Stretching with rotation - Finite element mesh and boundary conditions.

The stress evolution equation, also under rigid-viscoplastic material hypothesis, is approximated by

$$|\sigma_{11,22}| = (\sigma_y + A)\left(1 + 2\sqrt{\frac{3}{2}}\vartheta\frac{K^2t}{K^2t^2+1}\right)^{1/m}. \tag{63}$$

The comparisons between analytical and numerical for the stress and hardening evolution for different deformation rates are presented in Figs. 8 and 9. The results depicted in these figures show a very good agreement between the analytical and numerical data. As for the last two subsections a brick element was considered in the analysis, see the multiaxial solution.

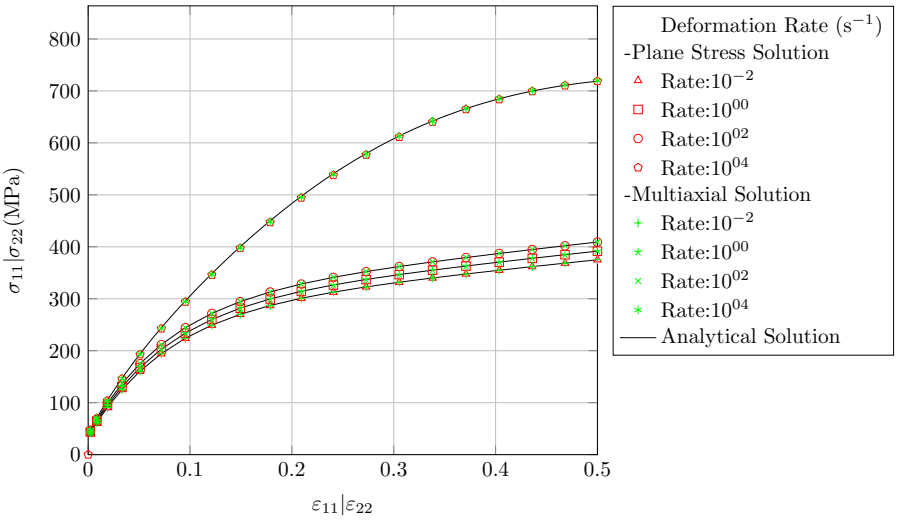

Figure 8: Comparison of flow stress-strain results viscoplastic strain for biaxial stretching with finite rotation.

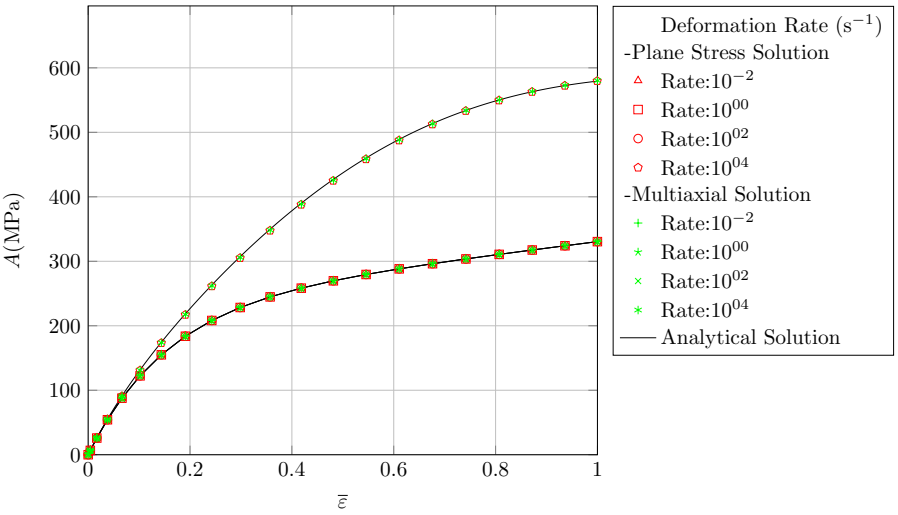

Figure 9: Comparison of hardening versus accumulated viscoplastic strain for biaxial stretching with finite rotation.

5.2 Stretching a perforated plate

This subsection describes an elasto-viscoplastic problem of a stretching of a perforated plate. Unlike the simple problems analyzed previously, which develop homogeneous stress-strain fields, in the present problem this does not happen.

5.2.1 Verification example using a rate-insensitive hardening

The idea here is to compare the numerical results achieved using the proposed framework with those already published by other authors who employed different strategies to

impose the plane stress state. After an extensive research in the bibliography, we found the *plane stress* numerical results for the *elasto-viscoplastic* problem of a stretching a perforated plate published by [5] and [6]. Accordingly [6] the numerical solution for this problem was achieved by using the *nested iteration algorithm* to impose the plane stress state, see [6], page 469, for more details. Therefore, such results serve as the reference solution for the implementation using the stress-projected algorithm presented in this work.

The model used for this analysis is shown in Fig. 10, in which the dimensions, boundary conditions, discretization and material properties are shown. Also in this figure, the hardening law employed by [5] and [6] is stated. The model was discretized with 576 triangular elements having three nodes per element. It was constructed by applying appropriate boundary conditions to reproduce symmetry conditions resulting in only one quarter of the plate. In this example the Perić overstress function was employed for analysis.

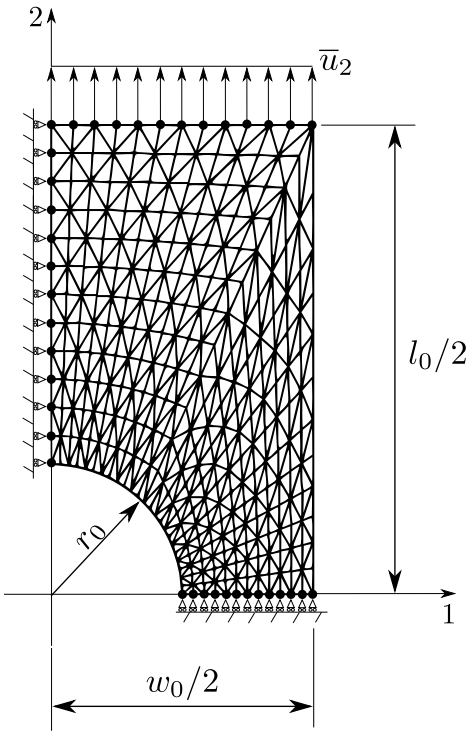

Geometry:
$w_0 = 20$ mm
$l_0 = 36$ mm
$r_0 = 5$ mm

Material properties:
$E = 70$ GPa
$\nu = 0.2$

Hardening law:
$\sigma_y(\overline{\varepsilon}) = 0.243 + 0.2\overline{\varepsilon}$ (GPa)

Viscosity parameter:
$\vartheta^{-1} = 0.002$ s^{-1}

Figure 10: Stretching of a perforated plate - Geometry, boundary conditions and finite element mesh.

For the hardening response to be compatible with the aforementioned publications, the parameters A_∞^{lwr} and A_∞^{up} were set to be unitary in Eq. (7), having $c = 0.2$ in Eq. (6). Also, the initial yield stress was set to $\sigma_y = 0.243$ in Eq. (1). Regarding the overstress function, it was necessary to multiply the parameter related to viscosity for the *Perić* model, ϑ, by $\sqrt{2/3}$. Such modification was necessary because the format of the equations in the cited works differs from the constitutive model used in this work.

The numerical analysis was carried out applying a total vertical displacement of $\overline{u}_2 = 6.15$ mm at the upper face of the plate, as shown in Fig. 10. Different constant rates were employed by varying the velocity v_2. The comparison with the works of [5] and [6] was established in terms of the reaction force in the direction 2 where the vertical displacement is prescribed. The total reaction force was obtained by the summation of the nodal reaction forces in the direction 2 considering loading rates varying from $2v_2/l_0 = 0.555\text{E}^{-4}$ to $2v_2/l_0 = 0.555\text{E}^{+2}$ s^{-1} for the cases where the exponent m in Eq. 28 is 1, 10 and 100.

In order to compare the results obtained in this work with those presented by [5] and [6], a careful digitization process was performed of the graphs presented by these respective authors. Then, with help of a software, we have extracted some data points on the curves from the digitization graph image. Of course, the process of digitization implies introducing some uncertainties in relation to the data obtained in comparison with the originals.

The comparison results for the stretching of the perforated plate are presented in terms of the total reaction force versus edge displacement in the graphs of Figs. 11, 12 and 13. Notice that, despite the uncertainties of the digitization process, the numerical results obtained with the proposed stress projected algorithm are very close to those presented by [5] and [6].

In addition to the rate dependent results we have also plotted the strain rate independent response in Figs. 11, 12 and 13 which was found using the present implementation, which serves as an illustrative and comparative feature of the proposed model. The rate independent case was model by increasing the exponent m to be a large value.

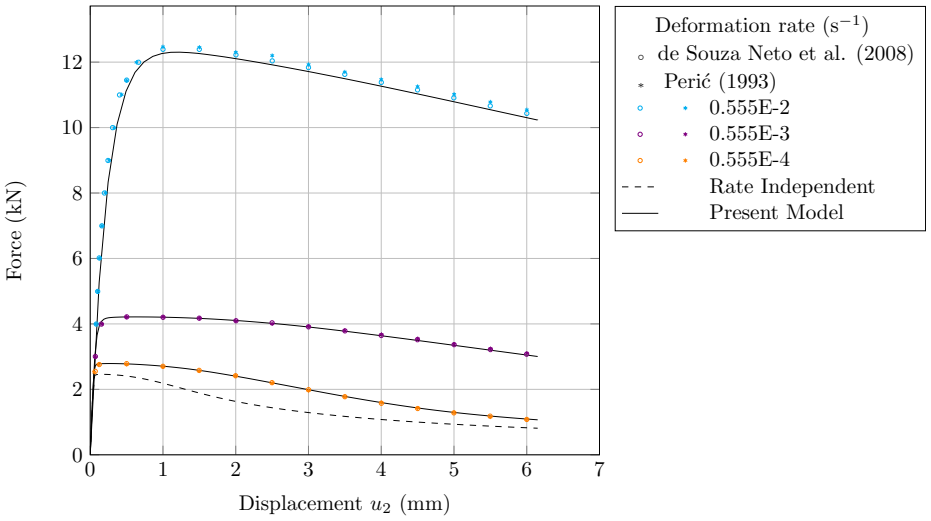

Figure 11: Results for stretching of a perforated plate - Force versus edge displacement for rate sensitivity exponent $m = 1$.

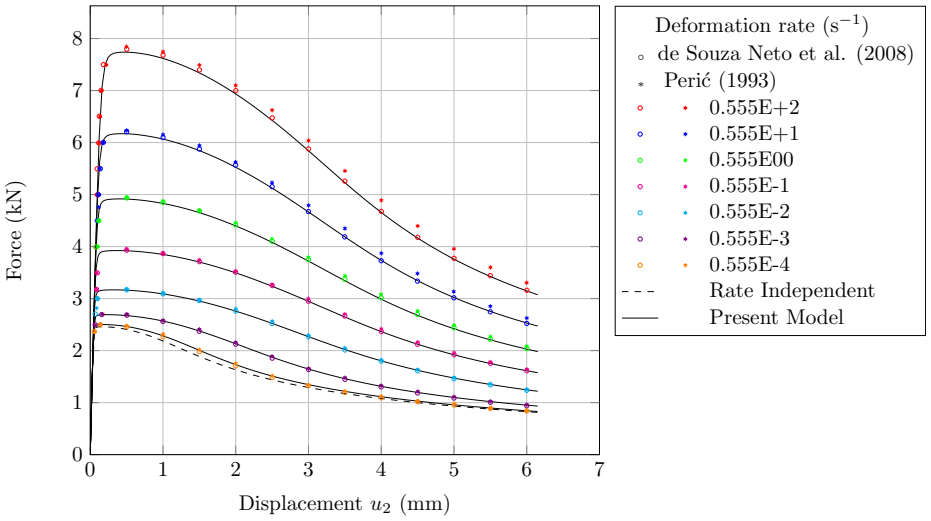

Figure 12: Results for stretching of a perforated plate - Force versus edge displacement for rate sensitivity exponent $m = 10$.

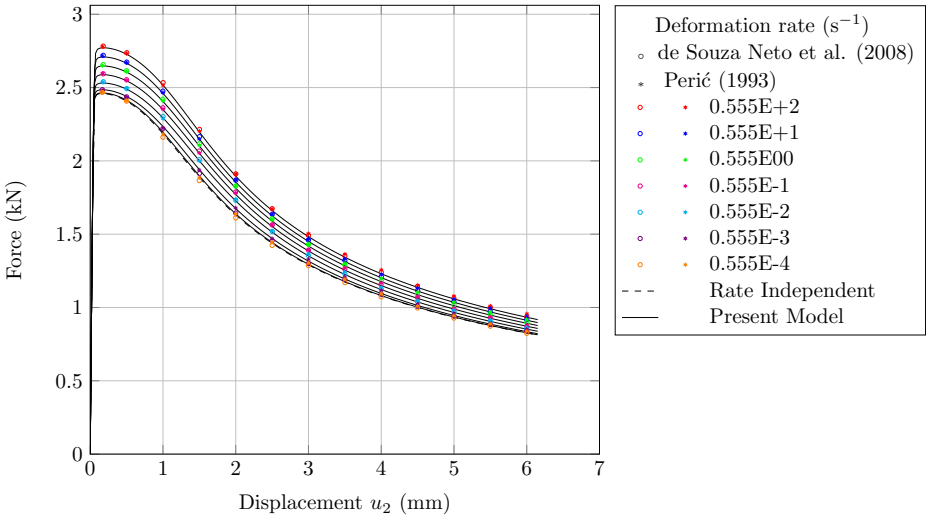

Figure 13: Results for stretching of a perforated plate - Force versus edge displacement for rate sensitivity exponent $m = 100$.

5.2.2 Rate-dependent hardening results

Now we turn our attention to the rate-dependent hardening effects on the response of components and structures. For this purpose, we consider the same discretization and boundary conditions shown in Fig. 10 but uses the full strain-rate hardening model described in subsection 2.1 together with the Perić overstress function Eq. (11) and the material parameters for OFHC cooper presented in Table 1.

The results for stretching of a perforated plate in terms of reaction force versus edge

displacement, for different rates of loading, and considering hardening strain-rate dependence and independence are presented in Fig. 14. Note that the higher the loading rate the greater is the difference between the formulations that consider strain-rate dependent hardening to that for which the hardening is insensitive to the strain-rate. For the higher rate consider in this case, 10^4 s^{-1}, this difference is high, showing the importance of such consideration in viscoplastic analysis of structures.

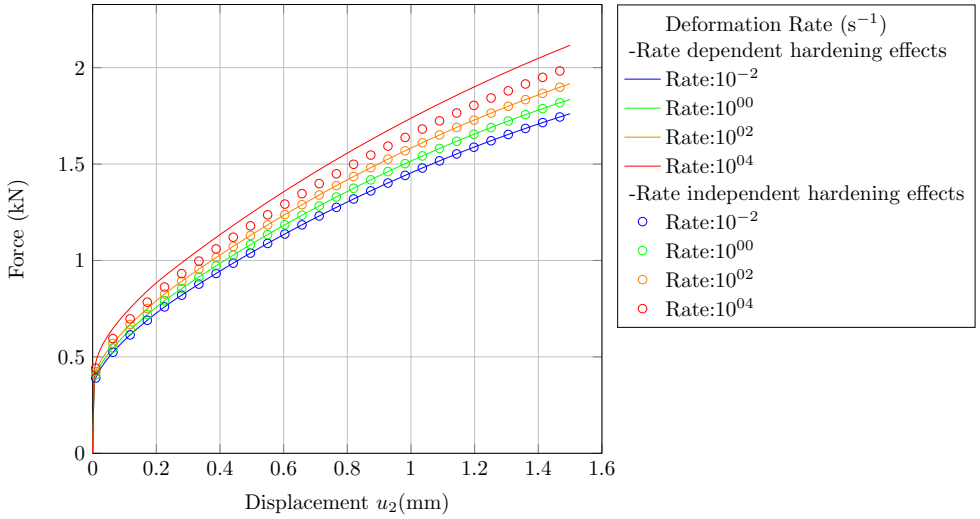

Figure 14: Results for stretching of a perforated plate - Force versus edge displacement for strain-rate dependence and independence hardening formulations.

6 CONCLUSIONS

This paper presented verification examples in elasto-viscoplasticity that shall be considered for code checking, a very important issue during the development of numerical algorithms and further implementation in the nonlinear world. Such verification examples were developed and used to verify the numerical accuracy and precision of an in-house implementation of the stress projected algorithm routines inside the context of elasto-viscoplasticity and the finite element method. During the studying and developing of own constitutive models for elasto-viscoplasticity we faced the necessity to check the program and noticed, quite surprisingly, that there are very few works in the literature treating of the imposition of the plane stress state inside the context of elasto-viscoplasticity. A version of the so-called stress-projected framework to enforce the plane stress state inside the context of viscoplasticity is presented in details. It has been demonstrated that this strategy can be used within the viscoplasticity approach provided that special attention is given to the treatment of the overstress function.

ACKNOWLEDGMENTS

The author Andrey Brezolin wishes to acknowledge the master scholarship supported by *CAPES*, Coordenação de Aperfeiçoamento de Pessoal de Nível Superior. The au-

thor Rodrigo Rossi wishes to acknowledge the support of *CNPq*, Conselho Nacional de Desenvolvimento Científico e Tecnológico (Grant number 306058/2018-9).

REFERENCES

[1] dos Santos, T. *Experimental characterization and constitutive modeling of a viscoplastic effects in high strain-rate deformation of polycrystalline FCC metals*. PhD thesis, Universidade Federal do Rio Grande do Sul, (2016).

[2] dos Santos, T., Rosa, P. A., Maghous, S., and Rossi, R. A simplified approach to high strain rate effects in cold deformation of polycrystalline fcc metals: Constitutive formulation and model calibration. *International Journal of Plasticity* **82**, 76 – 96 (2016).

[3] Perzyna, P. Fundamental problems in viscoplasticity. volume 9 of *Advances in Applied Mechanics*, 243–377. Elsevier (1966).

[4] Perzyna, P. Thermodynamic theory of viscoplasticity. volume 11 of *Advances in Applied Mechanics*, 313–354. Elsevier (1971).

[5] Perić, D. On a class of constitutive equations in viscoplasticity: Formulation and computational issues. *International Journal for Numerical Methods in Engineering* **36**(8), 1365–1393 (1993).

[6] de Souza Neto, E., Peric, D., and Owen, D. *Computational Methods for Plasticity: Theory and Applications*. Wiley, (2008).

[7] Schreyer, H. L., Kulak, R. F., and Kramer, J. M. Accurate numerical solutions for elastic-plastic models. *Journal of Pressure Vessel Technology* **101**(3), 226–234 (1979).

[8] Jetteur, P. Implicit integration algorithm for elastoplasticity in plane stress analysis. *Engineering Computations* **3**(3), 251–253 (1986).

[9] Simo, J. C. and Taylor, R. L. A return mapping algorithm for plane stress elastoplasticity. *International Journal for Numerical Methods in Engineering* **22**(3), 649–670 (1986).

[10] Hornberger, K. and Stamm, H. An implicit integration algorithm with a projection method for viscoplastic constitutive equations. *International Journal for Numerical Methods in Engineering* **28**(10), 2397–2421 (1989).

[11] Walz, G., Hornberger, K., and Stamm, H. An implicit integration algorithm for plane stress viscoplastic constitutive equations. *Computers & Structures* **36**(3), 539 – 546 (1990).

[12] Ohno, N., Tsuda, M., Sugiyama, H., and Okumura, D. Elastic-viscoplastic implicit integration algorithm applicable to both plane stress and three-dimensional stress states. *Finite Elements in Analysis and Design* **109**, 54 – 64 (2016).

[13] Paris, T. and Saanouni, K. Damaged behavior under plane stress. *European Journal of Computational Mechanics* **20**(5-6), 341–368 (2011).

[14] Lee, S., Yoon, J., and Yang, D. A stress integration algorithm for plane stress elastoplasticity and its applications to explicit finite element analysis of sheet metal forming processes. *Computers & Structures* **66**(2), 301 – 311 (1998).

[15] Valoroso, N. and Rosati, L. Consistent derivation of the constitutive algorithm for plane stress isotropic plasticity. part I: Theoretical formulation. *International Journal of Solids and Structures* **46**(1), 74 – 91 (2009).

[16] Valoroso, N. and Rosati, L. Consistent derivation of the constitutive algorithm for plane stress isotropic plasticity. part II: Computational issues. *International Journal of Solids and Structures* **46**(1), 92 – 124 (2009).

[17] Montáns, F. J. Implicit plane stress algorithm for multilayer j2-plasticity using the prager-ziegler translation rule. *International Journal for Numerical Methods in Engineering* **59**(3), 409–418 (2003).

[18] Simo, J. and Hughes, T. *Computational Inelasticity*. Interdisciplinary Applied Mathematics. Springer New York, (1998).

[19] Brezolin, A. Avaliação numérica de um modelo de viscoplasticidade com endurecimento dependente da taxa de deformação. Master's thesis, Universidade Federal do Rio Grande do Sul, (2018).